JOURNAL OF MATERIALS SCIENCE 38 (2003) 1195–1201

A model for austenitisation of hypoeutectoid steels

D. GAUDE-FUGAROLAS, H. K. D. H. BHADESHIA
Department of Materials Science and Metallurgy, University of Cambridge, Pembroke Street, Cambridge CB2 3QZ, UK

In the field of phase transformations in steels, much attention has been paid to the transformation of austenite into diverse product phases but, until recently not much work has been done on the formation of austenite during heating. There are few published models dealing with the transformation of eutectoid or hypoeutectoid steels with a starting microstructure which is a mixture of ferrite and pearlite.

The aim of the present work was to use phase transformation theory to develop a model for austenite formation which takes into account the chemical composition and microstructure of the steel studied, and thermal history experienced. Classic nucleation theory and diffusion-controlled growth equations are used to determine the progressive transformation of the different phases into austenite.

A phase transformation model with sound physical basis as the one presented in this work can be used to determine the effects of various parameters in the reaction involved, like microstructure (grain size, pearlite spacing), composition, heating rate and others. Another direct application of this model is the generation of CHT (continuous heating transformation) diagrams for specific steels, which are a useful reference in research, as well as in many industrial processes.

1. Introduction

In the field of phase transformations in steels, much attention has been paid to the transformation of austenite into diverse product phases but, until recently not much work has been done on the formation of austenite during heating [1–15]. There are some published models which deal with the transformation of eutectoid or hypoeutectoid steels with a starting microstructure which is a mixture of ferrite and pearlite [15–20].

The aim of the present work was to use phase transformation theory to develop a model for austenite formation which takes into account the chemical composition and microstructure of the steel studied, and thermal history experienced. Classic nucleation theory and diffusion-controlled growth equations are used to determine the progressive transformation of the different phases into austenite.

A model such as this may be useful in diverse applications, ranging from the calculation of continuous heating diagrams of steels of precise composition and microstructure, to the simulation and monitoring of manufacturing processes.

2. Austenitisation of a hypoeutectoid steel

The phenomenology of austenitisation of an hypoeutectoid steel is more complex than that of the same transformation in other alloys. The equilibrium microstructure is composed of ferrite and pearlite, the latter being a composite of ferrite and cementite. In two-dimensional sections a colony of pearlite has the appearance of alternate lamellae of ferrite and cementite. In three-dimensions each colony consists of an interpenetrating bi-crystal of ferrite (α) and cementite (θ) [21]. Ferrite has a very low solubility of carbon and hence, on its own, only begins to transform to austenite at high temperatures. But if cementite decomposes and yields its carbon to the transformation front, the reaction from ferrite to austenite can proceed at lower temperatures.

It is the logical to expect that the initiation of austenitisation in a hypoeutectoid steel is in pearlite, where the diffusion distances for carbon are small. The reaction can then proceed into the remaining ferrite once the pearlite is consumed.

New grains of austenite nucleate at pearlite colony boundaries [15]. As the diffusion distances for carbon from the dissolving cementite to the ferrite austenite interface are small (smaller or equal to half the spacing characteristic of the pearlite), these grains grow extremely fast, to the extent that pearlite is sometimes assumed to transform instantly [15] into austenite, followed by the advance of the interface into the ferrite.

When the austenite starts to grow into the ferrite, carbon has to partition to the austenite/ferrite interface for the reaction to proceed, so the diffusion rate of carbon in austenite becomes one of the limiting factors, but the range of this diffusion process is much larger and the rate of transformation will depend on the morphology, distribution and volume fractions of the phases present.

Any model aiming to describe reaustenitisation of an hypoeutectoid steel has to deal with all the parameters

referred to above. Austenitisation must clearly be microstructure sensitive. Thermodynamic equilibrium limits the extent of transformation at long times, while nucleation of austenite in pearlite colonies and diffusive processes are expected to control the rates of transformation.

The model described in this work includes nucleation of new austenite grains at the edges of the pearlite colonies. These grains will be assumed to grow until the pearlite has completely transformed into austenite, after which allotriomorphic ferrite transforms.

3. Characterisation of the microstructure

A hypoeutectoid carbon steel presents two distinctive microstructures, groups of pearlite colonies and some ferrite grains between them. This distribution of phases is even more accentuated in the case of steels containing chemical segregation, which on rolling lead to a banded structure.

If it is assumed that the latter is always the case, it is possible to define the microstructure of the steel using four independent parameters, as shown in Figs 1 and 2. In a more general microstructure, it is assumed that these parameters would still represent the extent of each phase (ignoring its internal microstructure) in a way which accounts for austenite formation.

The parameters l_α and l_p define the thickness of the ferrite and pearlite layers respectively. The sum of both gives l_h. In a structure that is not heavily banded, l_α and l_p are used in an abstract way to define the relative volume fractions of allotriomorphic ferrite and pearlite. Assuming that the carbon content of ferrite is zero, and that pearlite as a whole has the eutectoid carbon composition (0.77 wt%), l_p can be defined as,

$$l_p = \frac{l_h\, w_c}{0.77} \tag{1}$$

with

$$l_h = l_\alpha + l_p \tag{2}$$

where w_c is the weight percent of carbon.

The dimension of the pearlite colonies l_{col} may be defined as a typical colony diameter, as shown in Fig. 2, and it has been measured using the linear mean interception method. Finally, l_e characterises the eutectoid ferrite cementite periodicity.

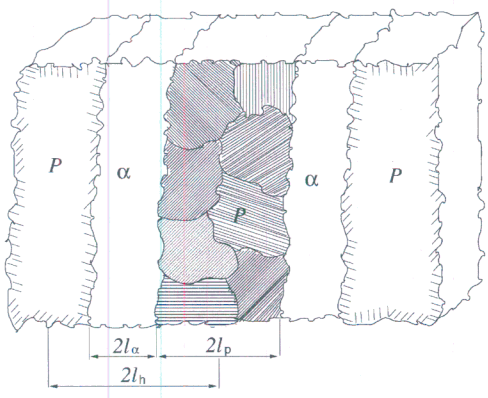

Figure 1 Definition of microstructure parameters l_p, l_α and l_h. *P* denotes pearlite regions and α the ferrite regions.

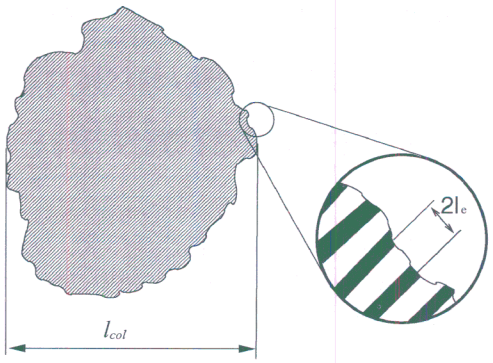

Figure 2 Definition of microstructure parameters l_{col} and l_e.

There is no need to define the thicknesses of the cementite and ferrite layers in pearlite because it is assumed here that both layers decompose into austenite at a common transformation front.

All the quantitative metallographic methods used during this study were conducted following Sellars [22] unless stated otherwise, and stereological corrections, when needed, were done as in Chang *et al.* [23].

4. Nucleation of austenite in pearlite colonies

Austenite nucleates at the surfaces of the pearlite colonies [15]. Classic nucleation theory [24] is used to calculate the dependence of nucleation on temperature.

$$I = C_0 N_0 \frac{6}{l_{\text{col}}} \frac{k\,T}{h} \exp\left(-\frac{G^* + Q}{R\,T}\right) \tag{3}$$

where I is the nucleation rate per unit time in a single colony, N_0 is the number of nucleation sites per unit area of colony interface, and C_0 is a fitting parameter. The active nuclei are all assumed to be located at the surface of the pearlite colonies; hence the ratio between colony surface to volume, which gives the factor $\frac{6}{l_{\text{col}}}$. k is the Boltzmann constant; R the gas constant; h the Planck constant; Q is an activation energy representing the barrier for the iron atoms to cross the interface, estimated to be 270,000 J mol^{-1} [25]. T is the absolute temperature and G^* is the activation free energy for nucleation.

The activation free energy for nucleation is determined from a balance of interface and volume energy of the critical nucleus. The austenite/ferrite interface energy at nucleation is considered to be $\gamma = 0.025$ J m^{-2} [25]. Several authors [26–29] have studied the effect of composition on the increase in free energy on transformation from ferrite to austenite, but not of cementite and ferrite to austenite. The increase in free energy from ferrite + cementite to austenite is determined as follows.

Such free energy can be estimated using commercial software such as MTDATA [30]. However, an analytical expression was designed in order to produce a stand-alone computer model. Therefore, a group of virtual experiments were designed, in which the composition was varied about an average value (Table I). Experiment design methods [31] have been used to determine the representative combinations. 32 different compositions have been considered, so that none of the 7 factors (element composition: Fe, C, Si, Mn, Cr, Ni, Mo) is

TABLE I Composition values used in the virtual experiments

	C (wt.%)	Si (wt.%)	Mn (wt.%)	Cr (wt.%)	Ni (wt.%)	Mo (wt.%)
Average	0.54	0.21	0.77	0.18	0.11	0.03
Level +	0.77	0.42	1.5	0.36	0.22	0.06
Level −	0.27	0.10	0.35	0.09	0.05	0.01

confused with others or interactions lower than the 4th degree. The higher and lower level of each composition corresponds to approximately twice and half the composition of the average steel. The average composition has also been added to the list of compositions used.

All these different steels were studied using MTDATA [30] in the temperature range 373–1873 K, in steps of 25 K, assuming paraequilibrium. The free energy change on transformation from ferrite and cementite to austenite was thus determined.

The data obtained from MTDATA were used to train a neural network, using software developed by Neuromat [32], based on the work done by MacKay [33, 34]. The network has 8 input variables (7 elements and temperature) and 13 hidden units. The analytical function thus created can then be incorporated into a stand-alone computer model.

5. Diffusion-controlled growth of austenite in steel

Once the new grains of austenite have nucleated, their rate of growth, up to the equilibrium volume fraction, has been assumed to be determined by the diffusion of carbon in austenite, from the decomposing cementite, to the boundary between ferrite and austenite. The velocity of that interface can be determined from a mass balance and the relevant diffusion equation.

The flux of carbon atoms in austenite at the ferrite/austenite interface is

$$D\left(\frac{\partial c}{\partial r}\right)_{r=r^{\text{int}}} \mathrm{d}t \tag{4}$$

where $D = D(c, T)$ is the diffusion coefficient of carbon in austenite; c the carbon content of the steel; and r^{int} the position of the interface.

The atoms involved in the boundary advance is determined by

$$(c^{\gamma\alpha} - c^{\alpha\gamma})\mathrm{d}r \tag{5}$$

where $c^{\gamma\alpha}$ and $c^{\alpha\gamma}$ are the composition of austenite and ferrite in paraequilibrium with each other close to the γ/α interface, and are calculated following Akbay *et al.* [7].

Equating Equations 4 and 5 gives

$$D\left(\frac{\partial c}{\partial r}\right)_{r=r^{\text{int}}} \mathrm{d}t = (c^{\gamma\alpha} - c^{\alpha\gamma})\mathrm{d}r \tag{6}$$

so that the velocity of the interface v_{int} can be determined as follows

$$v^{\text{int}} = \frac{\mathrm{d}r}{\mathrm{d}t} = \frac{D\left(\frac{\partial c}{\partial r}\right)_{r=r^{\text{int}}}}{(c^{\gamma\alpha} - c^{\alpha\gamma})} \tag{7}$$

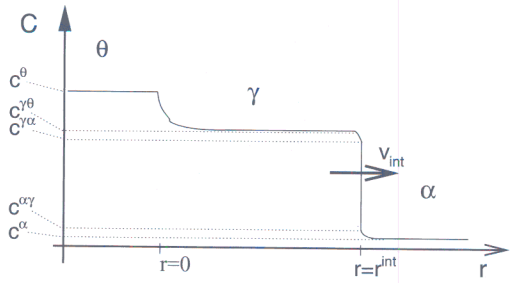

Figure 3 Carbon content and position of the interface.

The determination of the concentration gradient in a situation with moving boundaries (Stefan problem Fig. 3) doesn't have a simple solution [35]. Using the following approximation,

$$\left(\frac{\partial c}{\partial r}\right)_{r=r^{\text{int}}} \approx \left(\frac{c^{\gamma\theta} - c^{\gamma\alpha}}{r}\right) \tag{8}$$

the velocity of the interface can be calculated to be

$$v^{\text{int}} \approx \frac{D}{r}\left(\frac{c^{\gamma\theta} - c^{\gamma\alpha}}{c^{\gamma\alpha} - c^{\alpha\gamma}}\right) \tag{9}$$

Is important to note that r in Equation 9 is the diffusion distance of carbon in austenite, and that unless the direction of that flux and the direction of advancement of the interface are coincident the position of the interface will have to be determined as $v^{\text{int}}t$, where t is time.

6. Transformation of pearlite

The nucleation rate of austenite in a pearlite colony is I (Equation 3). Each active nucleus develops in one of the layers or "slices" of ferrite surrounded by cementite. The newly nucleated grains grow as hemispheres until they reach a size of the order of l_e and a steady growth rate, and start growing into the colony. If the geometry of the pearlite colony is assumed spherical, each ferrite layer is then a flat disc of radius R_1. As the new austenite grains grow from the edges of these discs (Fig. 4), the area already transformed can be accounted as

$$A = \frac{1}{2}\left[R_1^2(\theta_1 - \sin\theta_1) + R_2^2(\theta_2 - \sin\theta_2)\right] \tag{10}$$

where A is the area that has already transformed (using the average velocity of advance of the interface, see

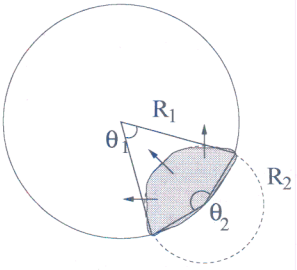

Figure 4 Transformed area (in grey) in a single *slice*.

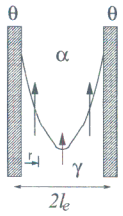

Figure 5 Interface profile within a *slice*.

below). R_1 is the radius of the slice and R_2 the position of the interface from the edge of the colony. θ_1 and θ_2 are the angles containing the transformed area from the centre of each circle.

In this case, the advancement direction of the interface is perpendicular to the diffusion of carbon. The velocity of the interface determined in section 5 is a function of the diffusion distance r. That obviously means that the advancing front of austenite will show different velocities from the α/θ interface to the centre of the ferrite lamina (Fig. 5). As the velocity of the interface is a function of the inverse of the diffusion distance, the interface would not be flat, but presents instead a double hyperbolic contour. In order to avoid increasing the complexity of the model, an average advance velocity for a flat interface is used.

The average advance velocity can be determined as

$$\bar{v}^{\text{int}} = \frac{1}{r_f - r_0} \int_{r_0}^{r_f} v^{\text{int}}\, \mathrm{d}r \tag{11}$$

$$\bar{v}^{\text{int}} = \frac{1}{r_f - r_0} \int_{r_0}^{r_f} \frac{1}{r} D \left(\frac{c^{\gamma\theta} - c^{\gamma\alpha}}{c^{\gamma\alpha} - c^{\alpha\gamma}} \right) \mathrm{d}r \tag{12}$$

$$\bar{v}^{\text{int}} = \frac{1}{r_f - r_0} \int_{r_0}^{r_f} \frac{1}{r}\, \mathrm{d}r\, D \left(\frac{c^{\gamma\theta} - c^{\gamma\alpha}}{c^{\gamma\alpha} - c^{\alpha\gamma}} \right) \tag{13}$$

$$\bar{v}^{\text{int}} = \frac{1}{r_f - r_0} (\ln r_f - \ln r_0)\, D \left(\frac{c^{\gamma\theta} - c^{\gamma\alpha}}{c^{\gamma\alpha} - c^{\alpha\gamma}} \right) \tag{14}$$

where $\bar{v}^{\text{int}}$ is the averaged velocity of the interface. r_f and r_0 are the limits of integration, being in this case the distance to the centre of the slice (position that will correspond to the slowest movement of the interface), and the minimum distance from cementite in which we could consider to have steady growth of austenite (in the model, this value has been taken as a few cell parameters in thickness, 10^{-8} m). The other parameters have already been defined in Section 5. As the slices have a regular thickness, the conversion from area to volume is trivial.

As in many cases not only one single austenite nucleus will start to grow, an extended to real volume correction has been used, following the method presented by Avrami [36–38] and Cahn [39],

$$v_\gamma = 1 - \exp(-v_e) \tag{15}$$

where v_γ is the real volume fraction and v_e is the extended one.

TABLE II Composition of steels used

	C (wt%)	Si (wt%)	Mn (wt%)	Cr (wt%)	Ni (wt%)	Mo (wt%)	V (wt%)
Steel A	0.55	0.22	0.77	0.20	0.15	0.05	0.001
Steel B	0.54	0.20	0.74	0.20	0.17	0.05	0.001

7. Transformation of ferrite

Once all the pearlite has been transformed to austenite, the α/γ interface keeps advancing into the ferrite grains until all the material has been reaustenitised. This interface is considered to be flat. The concentration profile at the α/γ interface during austenite growth remains that illustrated on the right hand side of Fig. 3. As the diffusion distances become larger, the velocity of the interface v^{int} (Equation 9), becomes smaller.

Ferrite grains are assumed to be flat plates, with an average thickness of $2\,l_\alpha$, so that there is no need to use an extended/real volume correction.

8. Implementation of the model

The theory described thus far has been stated in terms of *isothermal* transformation, whereas it is the continuous heating experiments which are of technological interest. To account for anisothermal transformation, the kinetic equations were discretised for implementation into a computer program. For a given heating history, the heating curve is then divided into small temperature intervals, in each of which the calculation is isothermal. The boundary conditions are then changed to be appropiate for the next temperature interval and similar calculations are repeated to generate the entire transformation behaviour during heating.

9. Comparison with experimental results

In order to compare the predictions of the model with the transformation behaviour of steel, a standard set of experiments have been designed. This set of experiments can then be used to compare the capability of the model to predict the effects of other parameters like composition and microstructure. A series of six experiments was conducted, in which samples of steels A and B (Table II) were heated at 50°C s^{-1} to the maximum temperatures 746, 773, 812, 750, 725 and 725°C, spending 2.4, 2.7, 3.9, 4.5, 1.5 and 151 seconds respectively, above the A_{c1} temperature. All the temperatures quoted are in the intercritical range so only partial

TABLE III Microstructure of steels used

	$2l_\alpha \pm \sigma$ (m)	$2l_p$ (m)	$l_e \pm \sigma$ (m)	$l_{\text{col}} \pm \sigma$ (m)
Steel A	$(2.55 \pm 1.36)\,10^{-6}$	6.38×10^{-6}	$(0.51 \pm 0.05)\,10^{-6}$	$(19.73 \pm 0.95)\,10^{-6}$
Steel B	$(1.85 \pm 0.97)\,10^{-6}$	4.34×10^{-6}	$(0.25 \pm 0.05)\,10^{-6}$	$(18.46 \pm 0.95)\,10^{-6}$

transformation is expected, although the extent of austenite varied from very little to almost complete transformation.

Experimental data had been collected using a dilatometer (Thermecmastor Z), using hollow steel samples following the thermal history described in these six experiments. The same thermal history and the composition and microstructural description of the samples (Table III) were fed into the model and its results compared with experimental data.

The six experiments on steel A, as described above, were used to determine the nucleation fitting parameter C_0, obtaining the value $C_0 N_0 = 1.5 \times 10^{-3}$ m^{-2}. The model was then tested using the standard set of experiments against two steels of different composition, and slightly different microstructure. As shown in Figs 6 and 7, the predictions of the model give an excellent description of the experiments.

This kind of model can then be used in multiple applications, not being the least important of them the calculation of CHT (continuous heating transformation) diagrams for any hypoeutectoid steel, taking into account its composition and microstructure, as the one in Fig. 8, calculated for steel B, or the final distribution of phases after a reaustenitisation heat treatment.

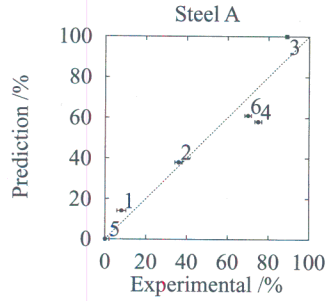

Figure 6 Predictions vs. experimental results on steel A.

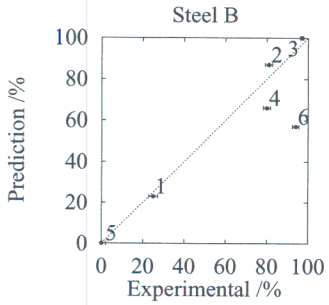

Figure 7 Predictions vs. experimental results on steel B.

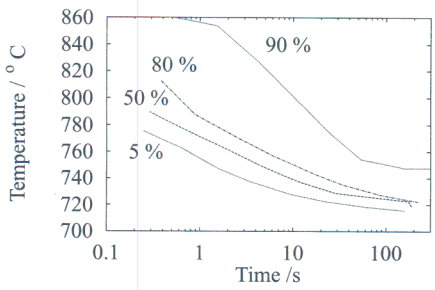

Figure 8 Continuous heating transformation diagram for steel B.

The CHT diagram shown in Fig. 8 was determined by feeding the model with 8 different constant heating rates (0.1, 0.3, 1, 3, 10, 30, 100, and 300°C s^{-1}) and the composition and microstructure of steel B.

10. Conclusions

A model describing the reaustenitisation of hypoeutectoid steel has been presented. A phase transformation model with sound physical basis as the one presented in this work can be used to determine the effects of various parameters in the reaction involved, like microstructure (grain size, pearlite spacing), composition, heating rate or even other parameters not included in the model at the moment, by comparison of experimental results with adequate predictions. Another direct application of this model is the generation of CHT (continuous heating transformation) diagrams for specific steels, which are a useful reference in research, as well as in many industrial processes.

Acknowledgements

We are grateful to GKNT Ltd. for financial support of this project. Special thanks are due to Dr. N. Hurd, Dr. G. Hollox and Dr. J. Garnham for their assistance in many phases of this project. Gratitude is expressed as well to Professor D. J. Fray FREng for the provision of laboratory facilities.

Appendix

The neural network described in section 4 has 8 input variables (7 elements and temperature) and one output variable (increase in volume free energy on transformation from ferrite/cementite mixtures to austenite). Both the input and output variables were first normalised within the range ±0.5 as follows:

$$x_N = \frac{x - x_{\min}}{x_{\max} - x_{\min}} - 0.5 \qquad (16)$$

where x_N is the normalised value of x, $x_{\max}$ the maximum value and $x_{\min}$ the minimum value of each variable of the original data. A similar operation was performed for the output variable. The maximum and minimum values of each of the inputs and output are summarised in Table IV.

TABLE IV Maximum and minimum values of each of the inputs and the output included in the database used to train the neural network

Variable (unit)	Minimum	Maximum
Fe (wt%)	0.9740	0.9913
C (wt%)	0.0027	0.0077
Si (wt%)	0.0010	0.0042
Mn (wt%)	0.0035	0.0077
Cr (wt%)	0.0009	0.0036
Ni (wt%)	0.0005	0.0022
Mo (wt%)	0.0001	0.0006
Temperature (K)	373	1873
Free energy (J m^{-3})	−14100	85900

The analytical function created during the neural network analysis has a standard feedforward network structure [40], with one hidden layer containing 13 hidden units. At every hidden unit j, each of the input variables x_i is multiplied by a coefficient (or *weight*) ($w_{j,i}^{(1)}$). All these products are then summed together and a constant (or *bias*) $\theta_j^{(1)}$ is added. The result of these operations is then used as the argument of a hyperbolic tangent.

$$h_j = \tanh\left(\sum_i w_{j,i}^{(1)} x_i + \theta_j^{(1)}\right) \qquad (17)$$

The normalised output is then calculated as,

$$y = \sum_j w_j^{(2)} h_j + \theta^{(2)} \qquad (18)$$

where $w^{(2)}$ is another weight and $\theta^{(2)}$ another bias respectively.

The values of the weights and biases of the function used are shown below. The data are arranged in a continuous horizontal sequence in the following order:

$$\begin{array}{llll} \theta_1^{(1)} & w_{1,1}^{(1)} & \cdots & w_{1,8}^{(1)} \\ \vdots & & & \\ \theta_{13}^{(1)} & w_{13,1}^{(1)} & \cdots & w_{13,8}^{(1)} \\ \theta^{(2)} & w_1^{(2)} & \cdots \quad \cdots & w_{13}^{(2)} \end{array}$$

−0.000927409	0.00225719	0.0359317	−0.0266119	0.00189785
0.00130568	−0.000127937	0.00442292	0.108438	
−0.706963	−0.0157156	−0.25495	0.0456821	0.00733509
−0.00257095	0.000431067	−0.000443135	5.06488	
0.374992	−0.00970058	−0.103038	−0.0146923	0.00819963
0.00505998	0.000343284	0.00382016	1.08423	
0.0161692	−0.000857959	−0.0194663	0.0128459	−0.00172985
−0.000458179	0.000123626	0.00131721	−0.0742627	
−1.10556	0.0191606	−0.00300155	0.00662053	−0.00824112
−0.000947285	−0.0016509	0.000137083	−2.22393	
0.414711	0.0140041	0.172736	−0.0378369	−0.00827716
0.00231805	−0.000638335	−0.0000687849	−4.5169	
0.166092	−0.00931884	−0.323855	−0.035193	0.0107671
0.00814719	−0.0016127	0.010268	0.305374	
−0.232182	0.0103279	0.0871771	−0.0239578	−0.015813
0.000866876	−0.000931361	−0.00111315	−4.77668	
0.0179458	0.0044031	0.0787807	−0.0434184	−0.00488125
0.00189372	−0.000959458	0.00403049	0.150206	
−0.404158	0.00147978	−0.303112	0.0330768	0.00111952
0.00243971	−0.000886333	0.00240586	1.59855	
−0.00475665	−0.00555445	−0.033777	0.0502044	0.00420753
−0.00113964	0.000137096	−0.00126711	−0.2042	
−0.50457	−0.00180787	0.0712752	0.116376	−0.00298373
−0.00644865	0.00238553	−0.0122309	0.0246812	
0.0852451	−0.0120447	−0.10675	0.0282623	0.0140425
−0.0016517	0.000774926	0.000709654	4.88308	
0.3815	−0.211064	0.844517	0.845746	0.10137
1.38627	1.56739	−0.756353	1.24645	−0.322463
0.456894	0.358231	−0.722532	1.75516	

References

1. R. MANCINI and C. BUDDE, *Acta Materialia* **47** (1999) 2907.
2. R. C. REED, T. AKBAY, Z. SHEN, J. M. ROBINSON and J. H. ROOT, *Materials Science and Engineering A* **256** (1998) 152.
3. R. C. REED, Z. SHEN, T. AKBAY and J. M. ROBINSON, *ibid.* **A232** (1997) 140.
4. G. A. ROBERTS and R. F. MEHL, *Transactions of the A.S.M.* **31** (1943) 613.
5. T. AKBAY and C. ATKINSON, *J. Mater. Sci.* **31** (1996) 2221.
6. *Idem., ibid.* **31** (1996) 5004.
7. T. AKBAY, R. C. REED and C. ATKINSON, *Acta Metallurgica et Materialia* **47** (1994) 1469.
8. A. ALI and H. K. D. H. BHADESHIA, *J. Mater. Sci.* **28** (1993) 3137.
9. C. ATKINSON and T. AKBAY, *Acta Materialia* **44** (1996) 2861.
10. C. ATKINSON, T. AKBAY and R. C. REED, *Acta Metallurgica Materialia* **43** (1995) 2013.
11. N. C. LAW and D. V. EDMONDS, *Metallurgical Transactions* A **11A** (1980) 33.
12. G. R. SPEICH, A. SZIRMAE and M. J. RICHARDS, *Transactions of the Metallurgical Society of A.I.M.E.* **245** (1969) 1063.
13. J. R. YANG and H. K. D. H. BHADESHIA, *Materials Science and Engineering A* **131** (1991) 99.
14. J. R. YANG and C. Y. HUANG, *Materials Chemistry and Physics* **35** (1993) 168.
15. C. R. BROOKS, "Principles of the Austenitization of Steels" (Elsevier Applied Science, London, 1992).
16. A. JACOT, M. RAPPAZ and R. C. REED, *Acta Materialia* **46** (1998) 3949.
17. A. JACOT and M. RAPPAZ, *ibid.* **45** (1997) 575.
18. *Idem., ibid.* **47** (1999) 1645.
19. F. G. CABALLERO, C. CAPDEVILA and C. GARCÍA DE ANDRÉS, *Scripta Materialia* **42** (2000) 1159.
20. C. GARCÍA DE ANDRÉS, F. G. CABALLERO, C. CAPDEVILA and H. K. D. H. BHADESHIA, *ibid.* **39** (1998) 791.
21. M. HILLERT, in "Decomposition of Austenite by Diffusional Processes," edited by V. F. Zackay and H. I. Aaronson, (Interscience, New York, 1962) p. 197.
22. C. M. SELLARS, Quantitative Metallography, Technical Report, Escuela Superior de Ingenieros Industriales de San Sebastian, 1981.

23. L. C. CHANG and H. K. D. H. BHADESHIA, *Materials Science and technology* **11** (1995) 874.
24. J. W. CHRISTIAN, "*Theory of Transformations in Metals and Alloys, Part I*" (Pergamon Press, Oxford, 1975).
25. S. J. JONES and H. K. D. H. BHADESHIA, *Metallurgical and Materials Transactions* A **28A** (1997) 2005.
26. C. ZENER, *Transactions of the A.I.M.E.* **203** (1955) 619.
27. L. KAUFMAN, E. V. CLOUGHERTY and R. J. WEISS, *Acta Metallurgica* **11** (1963) 323.
28. H. I. AARONSON, H. A. DOMIAN and G. M. POUND, *Transactions of the A.I.M.E.* **236** (1966) 768.
29. *Idem., ibid.* **236** (1966) 753.
30. S. M. HODSON, "MTDATA–Metallurgical and Thermochemical Databank" (National Physical Laboratory, Teddington, UK, 1989).
31. A. PRAT, X. TORT-MARTORELL and P. GRIMA, "Estadística teórica y Aplicada: Entregas 1 a 4" (C.P.D.A., Universitat Politècnica de Catalunya, Barcelona, 1992).
32. T. SOURMAIL, Neuromat Ltd., Models manager, 2000.
33. D. J. C. MACKAY, in "Mathematical Modelling of Weld Phenomena 3," edited by H. Cerjak (The Institute of Materials, London, 1997) p. 359.
34. D. J. C. MACKAY, "vised neural networks." available at http://wol.ra.phy.cam.ac.uk/mackay/.
35. J. CRANK, "The Mathematics of Diffusion" (Oxford University Press, Oxford, 1975).
36. M. AVRAMI, *Journal of Chemical Physics* **7** (1939) 1103.
37. *Idem., ibid.* **8** (1940) 212.
38. *Idem., ibid.* **9** (1941) 177.
39. J. W. CAHN, *Acta Metallurgica* **4** (1956) 449.
40. M. T. HAGAN, H. B. DEMUTH and M. BEALE, "Neural Network Design" (PWS Publishing, Boston, 1996).

Received 18 April
and accepted 25 November 2002